AEGC Australasian Exploration Geoscience Conference Brisbane 2021

The genesis and evolution of laminar carbonates in lacustrine basin: implications for shale oil accumulation

Chenyang Bai
School of Ocean Sciences,
China University of Geosciences (Beijing)
29th Xueyuan Rd., Haidian District,
Beijing 100083, P. R. China
baicy@cugb.edu.cn

Shujun Han
Department of Earth and Environmental Science,
Macquarie University
Sydney 2109,
Australia
cugbhansj@126.com

Zhenhuan Shen
School of Geosciences and Resources,
China University of Geosciences (Beijing)
29th Xueyuan Rd., Haidian District,
Beijing 100083, P. R. China
shenzh9311@163.com

SUMMARY

Shale oil has become a popular topic for global unconventional oil and gas research in the petroleum industry. Recent exploration efforts have indicated that laminar carbonates are closely related to the favorable depositional strata of lacustrine shale oil. This research focused on inter-bedded layers of laminar carbonates as well as mudstone and shale in the Dongying depression of the Bohai Bay Basin in eastern China, and attempted to reveal the genesis and evolution of the carbonates by petrological analyses. The results demonstrated that: the carbonates could be categorized into two groups, crystalline carbonates and micritic carbonates; the crystalline carbonates were well crystallized and greenish under fluorescent light; and the micritic carbonates were not well crystallized and had biotic textures. It was discovered that the crystalline carbonates were mainly developed in the shale layer and were formed from the late-filling effects of the diagenetic cracks along the shale fissility planes. The micritic carbonates were formed from direct deposition controlled by biological effects in the stratified flows of the seasonal lake basins. There are five main lithofacies in the study layers, which are as follows: LF1: thin lenticular laminae of crystalline carbonates, LF2: laminae of micritic carbonates, LF3: thick massive lime mudstone, LF4: massive mudstone, LF5: black shale. There are two shale oil accumulation models; one model commonly appears in LF4 and LF5 and is called "selfgeneration and self-reservoir"; the other model commonly appears in LF1 and is called the crystalline carbonate reservoir. Thus, the favorable lithofacies (assemblages) for shale oil accumulation are LF1, LF4 and LF5. In the petroleum industry, crystalline carbonates form "sweet spots", which are most beneficial for shale oil accumulation and production.

Key words: Carbonates, Lithofacies (assemblages), Shale oil, Dongying Depression, Bohai Bay Basin

INTRODUCTION

The development and utilization of shale oil and gas are the future of the fossil energy industry. In recent years, shale oil has received considerable attention as a new frontier in the petroleum industry (Holditch, 2013; Davies et al., 2014; Li et al., 2016a). Recent studies have concluded that shale oil in lacustrine basins, including the Green River Formation in the Uinta Basin and the Brown Shale in the Sumatra Basin, are promising targets for shale oil exploration and development (Burton et al., 2014; Schenk et al., 2015; Birdwell et al., 2016). Especially in lacustrine organic-rich mudrock layers, the mudrock that appears in many lacustrine basins is commonly carbonate dominated, such as the Araripe Basin in northeastern Brazil, the Ordos Basin in northwestern China, the Midland Valley Basin in Scotland, the Cankiri-Corum Basin in Turkey, the Santanghu Basin in northwestern China, and the Uinta Basin in the United States (Burton et al., 2014, Liu et al., 2015; Scherer et al., 2015; Li et al., 2016b; Merkel et al., 2016; Moradi et al., 2016), and the carbonate dominated shale even appears in some marine basins, such as the Sichuan Basin in southwestern China (Bristow et al., 2009). The carbonate components in mudrock layers not only exhibit uniform distribution but also appear as laminar structures, and both the content and structure of the carbonates exhibit significant variations in the vertical direction (Hao et al., 2014; Liang et al., 2017; Zhao et al., 2019). Some existing reports have indicated that many laminar carbonates occur in organic-rich mudrock layers are highly associated with shale oil reservoir (Hao et al., 2014; Hargrave et al., 2014; Liu et al., 2015; Wang et al., 2016; He et al., 2017). The genesis for laminar carbonate development in lacustrine basins incorporates the structural framework, water depth, lake chemistry and depositional environment; the structural framework provide stable deposition environment, lake chemistry and depositional environment control the mineral components, the enough water depth insure the laminar structure will not be destroy by strong hydrodynamic condition (Lerman et al., 1995; Martinek et al., 2006; Hargrave et al., 2014; Liu et al., 2015). However, meticulously analysis of the genesis for laminar carbonates in shale oil reservoir is rare. Thus, investigating, the relationship between laminar carbonates and shale oil accumulation is important for a correct understanding of lacustrine shale oil accumulation mechanism, which in turn is beneficial to the exploration and development of unconventional oil. The shale oil accumulation model constructed also could be utilized and referred in the world-wide shale oil exploration of similar basins.

The Dongying depression is a third-level tectonic unit within the Bohai Bay Basin in Eastern China where shale is well developed in Paleogene lacustrine sediments. Recent studies have shown that the Paleogene Shahejie Formation in the Dongying depression is an important reservoir of shale oil (Feng, et al., 2013; Cao et al., 2014; Hao et al., 2014; He et al., 2017). In recent years, some studies have demonstrated that there are substantial carbonate laminas interlaid within the organic-rich shale and mudstone sequence of the third and fourth members of the Shahejie Formation (Es_3-Es_4) in the Dongying depression (Feng, et al., 2013; Cao et al., 2014; Hao et al., 2014; He et al., 2017). We conducted petrological and geochemical studies based on the drill core samples from the Dongying depression. This paper reports the categorization of the different types of carbonates in the shale oil layers, discusses the genesis and depositional models of the carbonates.

Based above research, we characterized the various lithologies and lithologic assemblages of the shale oil reservoirs. In addition, we identified the genetic relationship between lithofacies (assemblages) and shale oil accumulation in lacustrine basins. Finally, we summarize the lithofacies (assemblages) that are favorable for shale oil accumulation, which could be used to predict the potential intervals and zones of shale oil.

METHOD AND RESULTS

Cores and thin sections

The core observations and samples used in this study were collected from wells Niuye1 and Fanye1 (Dongying depression) and well Luo69 (Zhanhua depression) in the Jiyang Sub-Basin (Fig. 1). These wells contained more organic-rich shale and claystone, and the core intervals of the study wells were consistently composed of the Es_3-3 to Es_4-1 members. Thin sections were prepared from the samples. Three pieces of sections were prepared at the same position in the same sample, one section for polarizing microscope and fluorescence microscope observation, the second for cathodoluminescence observation, and the third for scanning electron microscope (SEM) observation.

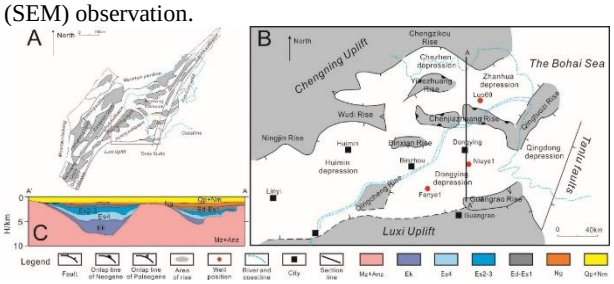

Figure 1. Geologic and section maps of the Jiyang Sub-Basin. A) structural map of the Bohai Bay Basin, where the red box outlines the Jiyang Sub-Basin. B) Tectonic setting of the Jiyang Sub-Basin; see C for detailed cross section of A-A′. C) Cross section A-A′ in B in the Jiyang Sub-Basin (modified from Feng et al., 2013).

Scanning electron microscope (SEM)

The sections of the samples were sprayed with a platinum conducting layer and were adopted for observation under a ZEISS S-3400N high-resolution field emission scanning electron microscope (FE-SEM) with ETH=15~20Kv and 30-μm aperture. An SE2 probe was adopted for observing the real microscopic features of the samples.

Cathodoluminescence (CL) Observations

The sections of the samples were cleaned and observed with a Leica CL8200 Cathodoluminescence Microscope with ETH=15kv. A high-sensitivity colored digital camera system associated with the CL microscope was used for photography.

Genesis of the crystalline carbonates

The crystalline carbonates occurred in different scales of lenticles with thicknesses from 1 mm to 3 mm and lengths from 5 mm to 150 mm interlayered in shale sequences. These crystalline carbonate lenticles were discontinuously distributed along the bed surfaces in shale to form one type of carbonate laminas (Fig. 2A, B). The crystalline carbonates mainly appeared light gray, gray, and grayish white and mainly consisted of calcite. The calcites within the crystalline carbonate lenticles appeared to have a euhedral-columnar texture perpendicular to the interfaces between the calcite crystals and shale (Fig. 2C, D). The columnar calcite demonstrated simple components and textures under the electron microscope, with a few internal pores, and showed a sharp boundary against the neighboring shale that consisted of clay minerals (Fig. 2E, F).

CL analysis showed that calcite crystals had dark red, bright red, orange and dark yellow luminescence. Different parts of the crystalline carbonate laminas had different color in luminescence. Calcite crystals in some samples showed oscillatory zoning under CL: the outer part of a calcite crystal had darker red luminescence than the inner part and showed bright red luminescence among the calcite crystals (Fig. 3A, B). Some edges of crystalline carbonate laminas showed bright red luminescence, and the inner crystalline carbonate laminas showed dark red luminescence (Fig. 3C, D). There were also some crystalline carbonate laminas that showed dark yellow luminescence, and only the middle parts of crystalline carbonate laminas showed orange luminescence (Fig. 3E, F).

Both the crystal morphology and oscillatory zoning under CL indicated that the bedding fissility in shale provided space for the growth of crystalline calcite. Therefore, all the lithological evidence demonstrates that the formation and derivation of the crystalline calcite were controlled by diagenesis and/or other post-depositional processes instead of sedimentation.

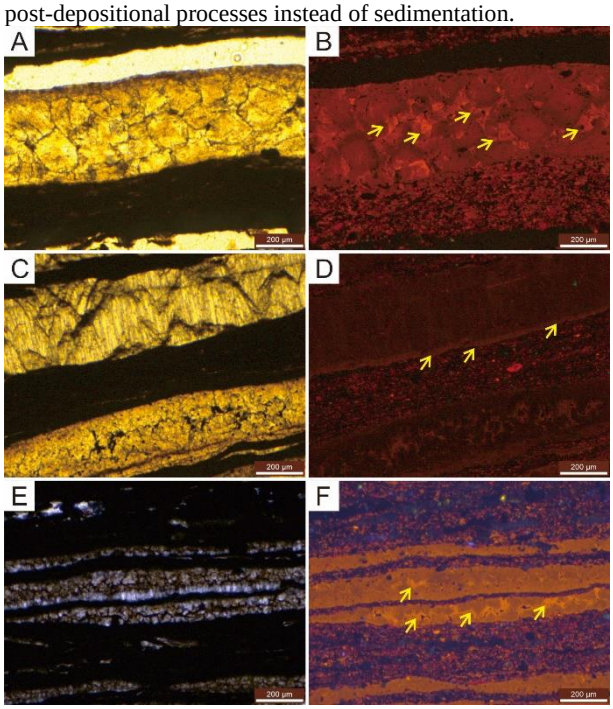

Figure 3. The cathodoluminescence photo of crystalline carbonates. A: well Niuye1, 3,458.57 m, plane-polarized light, carbonates with well-crystalline morphology; B: A under CL, yellow arrows indicate oscillatory zoning; C: well Fanye1, 3,418.47 m, plane-polarized light, crystalline carbonates showing euhedral-columnar texture; D: C under CL, yellow arrows indicate the edge of carbonate laminas that show bright red luminescence; E: well Niuye1, 3,458.57 m, plane-polarized light, carbonates with well-crystalline morphology; F: E under CL, yellow arrows indicated in middle part of crystalline carbonate laminas shows orange luminescence.

Genesis of the micritic carbonates

The micritic carbonates occurred in laminas with thicknesses from 1 mm to 3 mm interlayered in mudstone sequences. These micritic carbonate laminas were continuously distributed in mudstone layers (Fig. 4A, B). The micritic carbonates mainly appeared gray and deep gray and mainly consisted of micritic calcite grains. The micritic calcite grains in the form of badly crystallized fine grains (most diameters ≤ 4μm) and single grains were difficult to identify in cores and at thin section scale

(Fig. 3A-E). The micritic carbonate laminas had complex components; there was a mixture of a few clay and felsic minerals within the micritic carbonate laminas (Fig. 4C-E). The micritic carbonate laminas showed a transitional boundary against the neighboring mudstone that consisted of clay minerals (Fig. 4A-E). The micritic carbonate laminas were difficult to identify in cores and at thin section scale because of the calcite grains; therefore, micritic carbonate laminas were observed by SEM.

SEM testing on the micritic carbonates showed that the micritic carbonate laminas had relatively complicated inner textures. Badly crystallized calcite grains could be observed, mostly mixed with clay minerals (Fig. 5). Many biogenetic textures could be observed within the micritic carbonate laminas. Five patterns of textures were identified under the scanning electron microscope: (1) Spherical calcite above 1 μm in diameter. The spheres were smooth and regular on the surface and were isolated from each other (Fig. 5A). (2) Calcite with sheath-like texture, mostly in the shape of tubes or sheaths and mostly adhered with clay minerals and carbonates. Several sheath-like textures could be interwoven to form a frame structure (Fig. 5B, C). (3) Calcites with rod-like texture, mostly in the shape of rods or worms. These mainly accumulated to fill the space between the mineral grains (Fig. 5D). (4) Small spherical calcites. These were similar to the spherical calcite but the diameter was smaller, approximately 50 nm. They occurred either in single spheres or in bead-like or dumbbell-like aggregates of two or more calcite spheres (Fig. 5E). (5) Calcareous algae debris that occurred in a filamentary or ribbon-like shape; there were relatively few in the sample and they were mostly isolated from each other (Fig. 5F).

Micritic carbonates were also well developed in the studied wells. The micritic carbonates were predominantly calcites with poor crystallization mixed with a few clay minerals and felsic minerals. The micritic carbonate laminas were horizontally developed and mostly continuous. Moreover, the carbonate rocks showed a transitional boundary against the neighboring mudstone and shale layers. The evidence from petrology indicated that the carbonates were subject to sedimentation (Fig. 4A-E). Many biogenetic structures were observed under SEM: (1) Spherical minerals that mainly consisted of carbonates, especially calcites. This style of minerals could represent the process of biological control. Braissant et al. (2003) studied carbonate precipitates and made detailed descriptions of the features of carbonate crystals with and without amino acid joining. The spherical minerals were very similar to the carbonate crystals with amino acid as described by Braissant et al. (2003) (Fig. 5A). (2) Minerals with sheath-like texture that mainly consisted of carbonates, especially calcites. Since there were mixtures of some clay and felsic minerals in the micritic carbonate lamina, a few clay and felsic minerals were observed on the surface. These features represent biologically induced processes. Carbonate formation resulted from microbes such as cyanobacteria trapping (agglutination) sedimentary particles (Flügel, 2004). Several sheath-like textures could have been interweaved to form a net-like structure (Fig. 5B, C). The sheath-like carbonates found by Chafetz (1986) and Riquelme et al. (2015) were all very similar to the sheath-like texture found in this study (Fig. 5B-C). (3) Minerals with rod-like texture that mainly consisted of carbonates, especially calcites. These mainly accumulated to fill the space between the mineral grains. Riquelme et al. (2013) concluded that such rod-like minerals derived from a type of rod-like bacteria. The rod-like minerals found during this study were very similar to those of Riquelme et al. (2013) and may have been biologically induced (Fig. 5D). (4) EPS (Extracellular Polymeric Substances) textures. EPS accumulated outside the cells to form a protective and adhesive matrix that attached microbes to the substrate (Flügel, 2004). Based on the study of the pre-Cambrian Tarim Basin of You et al. (2013), spherical textures, dumbbell textures and bead-like textures of metastable nanometer crystalline carbonates, collectively known as EPS, were likely formed in microbe-rich water environments. The nanometer spherulitic textures found in this study were very similar to the EPS textures (Fig. 5E). (5) Minerals with irregular textures. A few irregular carbonate textures were found in the samples, mainly consisting of ribbon-shaped calcites (Fig. 5F). Qin et al. (2010) also found carbonates with similar textures in the organic-rich shale in Southern China and identified them as algal debris. The above-mentioned five carbonate textures all indicate that the formation of the carbonates was closely associated with microbes and biological effects. Additionally, the results of fluorescence microscopic observations showed that the micritic carbonate laminas had two different patterns. One pattern was that all the micritic carbonate laminas appeared greenish under fluorescent light (Fig. 4F, G). This pattern may indicate that the formation of the carbonates was effected by biological control and/or was biologically induced; this type of carbonate is autochthonous micrite (Flügel, 2004). Another pattern was that some aggregations scattered within the micritic carbonate laminas showed greenish under fluorescent light (Fig. 4H, I). This pattern may indicate that the carbonates were formed from the disintegration of benthic biota and/or pelagic biota; this type of carbonate is allochthonous micrite (Flügel, 2004).

The classification of lithofacies (assemblages)

Because the mineral constituents and sedimentary structure exhibit extensive variations, in this case, it is difficult to use the lithology as an indicator of shale oil accumulation. For example, the crystalline carbonate lenticles and laminar micritic carbonate are frequently interbedded with mudrocks in the research layers, and the carbonate content of the interbedded layers are higher than that of the pure mudrock layers. Thus, the vertical variation of carbonate content changes at a sub-meter scale. In addition, the same mineral constituents with different crystallized morphologies or sedimentary structures represent different genesis. Mudrocks with uniform micritic carbonates are normally associated with semi-deep lake environments (Flügel, 2004), and mudrocks interbedded with crystalline carbonate lenticles and laminar micritic carbonate are controlled by diagenesis and sedimentogenesis, respectively (Liu et al., 2019; Zhao et al., 2019). Even claystone and shale are controlled by different sedimentary environments (Ilgen et al., 2017). All the above differences in lithology, crystallized morphology, and sedimentary structures and conditions can be represented by lithofacies (assemblages) and can influence shale oil accumulation (Liang et al., 2017, 2018).

Based on the mineral compositions and genesis, lithologies, and sedimentary structures and conditions, eight lithofacies (assemblages) were identified in Es3-3 and Es4-1, and they are described in further detail below. Lithofacies assemblage 1+5 (LF1+5) is characterized by thin lenticular laminae of crystalline carbonate with black shale. Lithofacies assemblage 2+3 (LF2+3) is characterized by laminae of micritic carbonate with massive lime mudstone. Lithofacies 3 (LF3) is a thick massive lime mudstone. Lithofacies 4 (LF4) is massive claystone. Lithofacies 5 (LF5) is black shale. Lithofacies 6 (LF6) is massive siltstone. Lithofacies 7 (LF7) is characterized by laminae of siltstone. Lithofacies 8 (LF8) is massive gypsum.

Effects of Lithofacies on Shale Oil Accumulation

The sedimentary environments represented by different lithofacies (assemblages) are not consistent. The sedimentary environment represented by LF1+5 and LF5 has deeper water depth and weaker hydrodynamic conditions than those

represented by other lithofacies (assemblages). The LF4 also appears in a deep lake environment, but its water depth and hydrodynamic conditions are slightly shallower and stronger than LF1+5 and LF5 (Fig. 6). The sedimentary environments represented by LF2+3 and LF3 are obviously shallower than those of LF1+5, LF4 and LF5 (Fig. 6). The LF6, LF7 and LF8 represented the shallowest water depth (Fig. 6). The difference of sedimentary environment obviously affects the enrichment degree of organic matter. Based on analyses of sedimentary environments, deep water and reducing environments are beneficial to organic matter enrichment (Fig. 6A). Thus, in the study area, the evolution of the lacustrine shale oil begins in a semi-deep to deep lake environment in which LF1+5, LF4, and LF5 form (Fig. 6A). The migration and accumulation of hydrocarbons could occur via two different models, which are exemplified by LF1+5 and LF4/LF5. The massive claystone (LF4) and black shale (LF5) indicate deep and reducing environments with low deposition rates, and these environments are beneficial to organic matter enrichment (Wilkin and Barnes, 1997; Loucks and Ruppel, 2007). However, pure claystone and shale have massive structures with little porosity and permeability, and the large-scale migration of hydrocarbon in claystone and shale is very difficult. Thus, the hydrocarbons are primarily generated within LF4 and LF5, but they are adsorbed onto the clay minerals in these lithofacies, leading to in-situ accumulation with little migration (Elert et al., 2015; Sun et al., 2017; Zou, 2017). This is termed the "in-situ generation and in-situ reservoir (GR)" model (Fig. 6B).

The second model relies on the unique characteristics of the LF1+5 lithofacies assemblages, which are considerably heterogeneous, with crystalline carbonates interbedded with shale layers that have favorable fissile bedding. Most of the fissile bedding is distributed along weak stress surfaces controlled by the alignment of clay minerals (Fig. 6C). During diagenesis, the small-scale fissile bedding coalesces into a large space, and the crystalline carbonates form through dehydration of the clay minerals. Further, Ca-rich flows discharge through the area, causing fluid over-pressurization (Fig. 6C) (Guo et al., 2010). This is because the formation process of crystalline carbonates is controlled by diagenesis, not by sedimentation. The crystalline carbonates usually appear in black shale layers. Thus, LF1+5 also indicates deep and reducing environments with low deposition rates, which is beneficial to organic matter enrichment. The fissility of the shales provides considerable space, and these spaces are used for the crystallization of carbonates. However, they are also important for the migration and accumulation of hydrocarbons. Abundant fissile bedding of the shales in LF1+5 means that the hydrocarbons generated in LF5 can migrate into fissile bedding space over very short distances, and the fluid over-pressurization can accelerate the rate at which hydrocarbons migrate into the fissile bedding space of the shales. In addition, the large number of interparticle pores in the crystalline carbonates provides additional space for hydrocarbon accumulation. In the LF1+5 assemblage, hydrocarbons are generated within the shale layers adjacent to the crystalline carbonates. These hydrocarbons migrate short distances to the crystalline carbonates. Thus, some shale oil accumulates in the crystalline carbonates within LF1+5. In this model, the crystalline carbonates act as a shale oil reservoir, which herein is called the "crystalline carbonates reservoir (CCR)" model (Fig. 6C).

Herein, the CCR and GR models were compared; the former has more advantages than the GR model. The two models have similar abilities to generate hydrocarbons, and the LF1+5 of the CCR model has better reservoir space. In the layers studied in this work, pure LF4 and LF5 were rare, and LF1+5 dominated. Thus, the CCR model is the main reservoir model in the study area. Although some hydrocarbons remained in the shale part of LF1+5, the crystalline carbonates in LF1+5 still could indicate a favorable shale oil reservoir. Thus, LF1+5 is the most favorable lithofacies assemblage for shale oil accumulation.

CONCLUSIONS

Interlayers of mudrock and carbonates developed in the main oil source beds (Es_3-3 to Es_4-1) in the Dongying depression. The carbonates can be categorized into two groups: the micritic carbonates and the crystalline carbonates. The crystalline carbonates mainly developed in the diagenetic cracks and bedding fissility of shale because of the filling and crystallization of calcites from the diagenetic fluids. The micritic carbonates are mainly from direct sedimentation controlled by biological activities under the effects of seasonal lake water stratification. During the deposition of the Es_3-3 to Es_4-1 sub-members, five mainly lithofacies (assemblages) were formed in the study area. The analyses described here indicate that shale oil accumulation occurs via two models within the study area. The first model is the "crystalline carbonate reservoir (CCR)" model, which is exemplified by LF1+5. The second model is the "in-situ generation and in-situ reservoir (GR)" model, which is exemplified by LF4 and LF5. The LF1+5 is the most favourable lithofacies for shale oil accumulation.

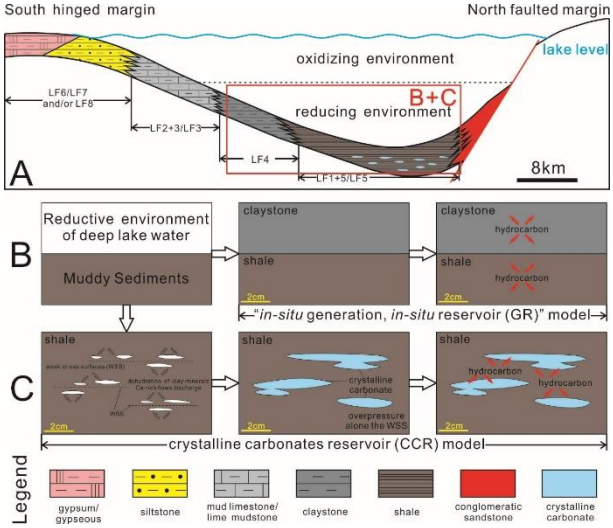

Figure 6. Model of the distribution and evolution of the lithofacies (assemblages) that are favorable for shale oil accumulation and storage.

ACKNOWLEDGMENTS

Our thanks should go to the Shengli Oilfield Company of SINOPC Group for their support in sample collection, rock core observation and data collection. Our thanks also go to Dr. Zhang Zhichao and Ph.D. candidates Ye Ruochen and Li Bo, MA. Sc Zhang Liyuan and Yang Bingfang for their support in field support, thin section identification and TOC test. Our thanks also go to Dr. Tian Y. Dong for his constructive comments. This work was supported by the National Science and Technology Major Project of China [Grant No. 2017ZX05049-004], National Program on Key Basic Research Project of China (973 Program) [Grant No. 2014CB239102], Chinese Fundamental Research Funds for the Central Universities [Grant No. 2652019079] and National Nature Science Foundation of China (General Program) [Grant No. 41572134].

REFERENCES

Braissant, O., Cailleau, G., Dupraz, C., Verrecchia, A.P., 2003. Bacterially induced mineralization of calcium carbonate in terrestrial environments: The role of exopolysaccharides and amino acids. J Sediment Res 73, 485-490.

Birdwell, Justin E, Berg, Michael D. Vanden, Johnson, Ronald C. et al. 2016. Geological, geochemical and reservoir characterization of the Uteland Butte member of the Green River Formation, Uinta Basin, Utah.

Bristow, T. F, Kennedy, M. J, Derkowski A. 2009. Mineralogical constraints on the paleoenvironments of the Ediacaran Doushantuo Formation. Proc. Natl. Acad. Sci. 106 (32): 13190-13195.

Burton, D., Woolf, K., and Sullivan, B. 2014. Lacustrine depositional environments in the Green River Formation, Uinta Basin: Expression in outcrop and wireline logs. AAPG Bull. 98 (9): 1699-1715.

Cao, Y. C., Yuan, G. H., Li, X. Y. et al. 2014. Characteristics and origin of abnormally high porosity zones in buried Paleogene clastic reservoirs in the Shengtuo area, Dongying Sag, East China. Pet. Sci. 11 (3): 346-362.

Chafetz, H.S., 1986. Marine Peloids - a Product of Bacterially Induced Precipitation of Calcite. J Sediment Petrol 56, 812-817.

Davies, R. J., Almond, S., Ward, R. S. et al. 2014. Oil and gas wells and their integrity: Implications for shale and unconventional resource exploitation. Mar. Pet. Geol. 56: 239-254.

Elert, K., Sebastian Pardo E., and Rodriguez-Navarro, C. 2015. Influence of organic matter on the reactivity of clay minerals in highly alkaline environments. Appl. Clay Sci. 111: 27-36.

Feng, Y. L., Li, S. T., and Lu, Y. C. 2013. Sequence stratigraphy and architectural variability in Late Eocene lacustrine strata of the Dongying Depression, Bohai Bay Basin, Eastern China. Sediment. Geol. 295: 1-26.

Flügel, Erik 2004. Microfacies of carbonate rocks-analysis, interpretation and application, Springer Berlin.

Guo, X. W., He, S., Liu, K. Y. et al. 2010. Oil generation as the dominant overpressure mechanism in the Cenozoic Dongying depression, Bohai Bay Basin, China. AAPG Bull. 94 (12): 1859-1881.

Hao, Y. Q., Chen, F. K., Zhu, J. Q. et al. 2014. Reservoir space of the Es33–Es41 shale in Dongying sag. International Journal of Mining Science and Technology 24 (4): 425-431.

Hargrave, J.E., Hicks, M.K., Scholz, C.A., 2014. Lacustrine Carbonates from Lake Turkana, Kenya: A Depositional Model of Carbonates in an Extensional Basin. J Sediment Res 84, 224-237.

He, J. H., Ding, W. L., Jiang, Z. X. et al. 2017. Mineralogical and chemical distribution of the Es3L oil shale in the Jiyang Depression, Bohai Bay Basin (E China): Implications for paleoenvironmental reconstruction and organic matter accumulation. Mar. Pet. Geol. 81: 196-219.

Holditch, Stephen A. 2013. Unconventional oil and gas resource development – Let's do it right. Journal of Unconventional Oil and Gas Resources 1–2: 2-8.

Ilgen, A. G., Heath, J. E., Akkutlu, I. Y. et al. 2017. Shales at all scales: Exploring coupled processes in mudrocks. Earth-Sci. Rev. 166: 132-152.

Lerman, A., Imboden, D. M., Gat, J., & Chou, L., 1995. Physics and chemistry of lakes. Physics and chemistry of lakes. Springer-Verlag.

Li, J., Zhou, S. X., Li, Y. J. et al. 2016a. Effect of organic matter on pore structure of mature lacustrine organic-rich shale: A case study of the Triassic Yanchang shale, Ordos Basin, China. Fuel 185: 421-431.

Li, S. F., Hu, S. Z., Xie, X, N. et al. 2016b. Assessment of shale oil potential using a new free hydrocarbon index. Int. J. Coal Geol. 156: 74-85.

Liang, C., Jiang, Z. X., Cao, Y. C. et al. 2017. Shale oil potential of lacustrine black shale in the Eocene Dongying depression: Implicationsfor geochemistry and reservoir characteristics. AAPG Bull. 101: 1835-1858.

Liang, C., Wu, J., Jiang, Z. X. et al. 2018. Sedimentary environmental controls on petrology and organic matter accumulation in the upper fourth member of the Shahejie Formation (Paleogene, Dongying depression, Bohai Bay Basin, China). Int. J. Coal Geol. 186: 1-13.

Liu, B., Lu, Y. F., Meng, Y. L. et al. 2015. Petrologic characteristics and genetic model of lacustrine lamellar fine-grained rock and its significance for shale oil exploration: A case study of Permian Lucaogou Formation in Malang sag, Santanghu Basin, NW China. Petroleum Explor. Dev. 42 (5): 656-666.

Liu, H. M., Zhang, S., Song, G. Q. et al. 2019. Effect of shale diagenesis on pores and storage capacity in the Paleogene Shahejie Formation, Dongying Depression, Bohai Bay Basin, east China. Mar. Pet. Geol. 103:738-752.

Loucks, R. G. and Ruppel, S. C. 2007. Mississippian Barnett Shale: Lithofacies and depositional setting of a deep-water shale-gas succession in the Fort Worth Basin, Texas. AAPG Bull. 91 (4): 579-601.

Martínek, K., Blecha, M., Daněk, V., Franců, J., Hladíková, J., & Johnová, R., et al., 2006. Record of palaeoenvironmental changes in a lower permian organic-rich lacustrine succession: integrated sedimentological and geochemical study of the rudník member, krkonoše piedmont basin, czech republic. Palaeogeography Palaeoclimatology Palaeoecology, 230(1), 85-128.

Merkel, A., Fink, R., and Littke, R. 2016. High pressure methane sorption characteristics of lacustrine shales from the Midland Valley Basin, Scotland. Fuel 182: 361-372.

Moradi, A. V., Sari, A., and Akkaya, P. 2016. Paleoredox reconstruction of bituminous shales from the Miocene Hancili Formation, cankiri-corum Basin, Turkey: Evaluating the role of anoxia in accumulation of organic-rich shales. Mar. Pet. Geol. 78: 136-150.

Qin, J., Shen, B., Fu, X., Tao, G., Teng, G., 2010. Ultramicroscopic organic petrology and potential of hydrocarbon generation and expulsion of quality marine source rocks in South China. Oil & Gas Geology 31, 826-837. (In Chinese with English abstract)

Riquelme, C., Hathaway, J.J.M., Dapkevicius, M.D.N.E., Miller, A.Z., Kooser, A., Northup, D.E., Jurado, V., Fernandez, O., Saiz-Jimenez, C., Cheeptham, N., 2015. Actinobacterial Diversity in Volcanic Caves and Associated Geomicrobiological Interactions. Front Microbiol 6.

Riquelme, F., Alvarado-Ortega, J., Ruvalcaba-Sil, J.L., Aguilar-Franco, M., Porras-Muzquiz, H., 2013. Chemical fingerprints and microbial biomineralization of fish muscle tissues from the Late Cretaceous Muzquiz Lagerstatte, Mexico. Rev Mex Cienc Geol 30, 417-435.

Schenk, C. J., Charpentier, R. R., Klett, T. R. et al. 2015. Assessment of shale-oil resources of the Central Sumatra Basin, Indonesia, 2015. Fact Sheet.

Scherer, C. M. S., Goldberg, K., and Bardola, T. 2015. Facies architecture and sequence stratigraphy of an early post-rift fluvial succession, Aptian Barbalha Formation, Araripe Basin, northeastern Brazil. Sediment. Geol. 322: 43-62.

Sun, M. D., Yu, B. S., Hu, Q. H. et al. 2017. Pore connectivity and tracer migration of typical shales in south China. Fuel 203: 32-46.

Wang, Y., Wang, X., Song, G., Liu, H., Zhu, D., Zhu, D., Ding, J., Yang, W., Yin, Y., Zhang, S., Wang, M., 2016. Genetic connection between mud shale lithofacies and shale oil enrichment in Jiyang Depression, Bohai Bay Basin. Petrol Explor Dev+ 43, 696-704. (In Chinese with English abstract)
Wilkin, R. T. and Barnes, H. L. 1997. Formation processes of framboidal pyrite. Geochim. Cosmochim. Acta 61 (2): 323-339.
You, X.L., Sun, S., Zhu, J.Q., Li, Q., Hu, W.X., Dong, H.L., 2013. Microbially mediated dolomite in Cambrian stromatolites from the Tarim Basin, north-west China: implications for the role of organic substrate on dolomite precipitation. Terra Nova 25, 387-395.
Zhao, K., Du, X. B., Lu, Y. C. et al. 2019. Are light-dark coupled laminae in lacustrine shale seasonally controlled? A case study using astronomical tuning from 42.2 to 45.4 Ma in the Dongying Depression, Bohai Bay Basin, eastern China. Palaeogeogr. Palaeoclimatol. Palaeoecol. 528: 35-49.
Zou, C. N. 2017. Chapter 10 - Shale Oil and Gas. In Unconventional Petroleum Geology (Second Edition), 275-321. Elsevier.

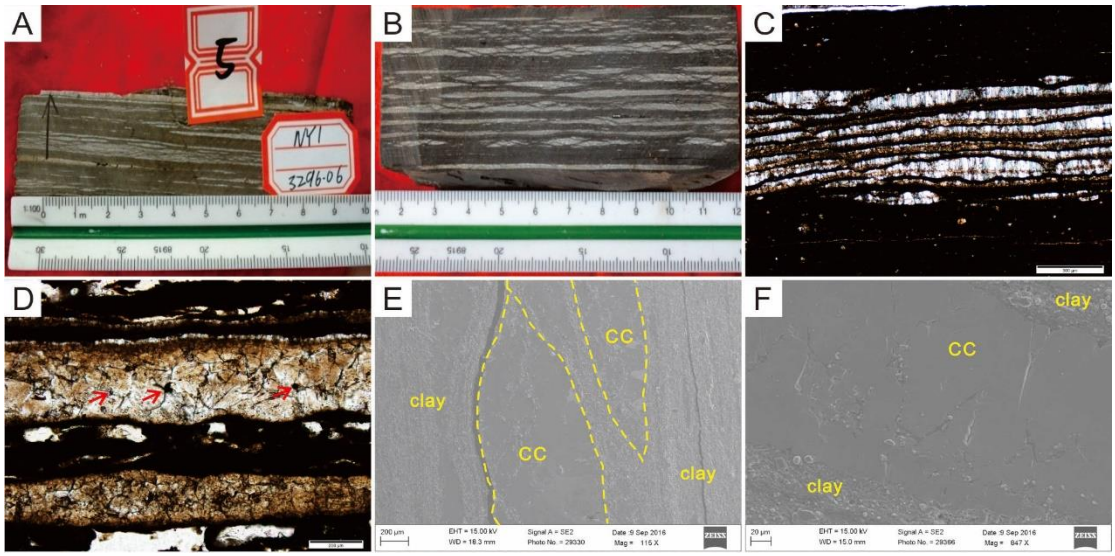

Figure 2. Crystalline carbonates. A: well Niuye1, 3,296.06 m, core photo, interbedded mudstone and shale and crystalline carbonate; B: well Fanye 1, 3,436.24 m, core photo, interbedded mudstone and shale and crystalline carbonate; C: well Niuye1, 3,414.23 m, cross-polarized light, crystalline carbonate layers show obvious lenticular features and carbonates show euhedral-columnar texture; D: well Niuye1, 3,458.57 m, cross-polarized light, crystalline carbonates shows well crystalized morphology, red arrows indicate organic matter filling the pores among the calcite crystals; E: well Fanye1, 3,413.44 m, SEM image, crystalline carbonates show lenticular features; F: well Niuye1, 3,316.00 m, SEM image, carbonates show euhedral-columnar texture and are well crystallized and clean on the surface.

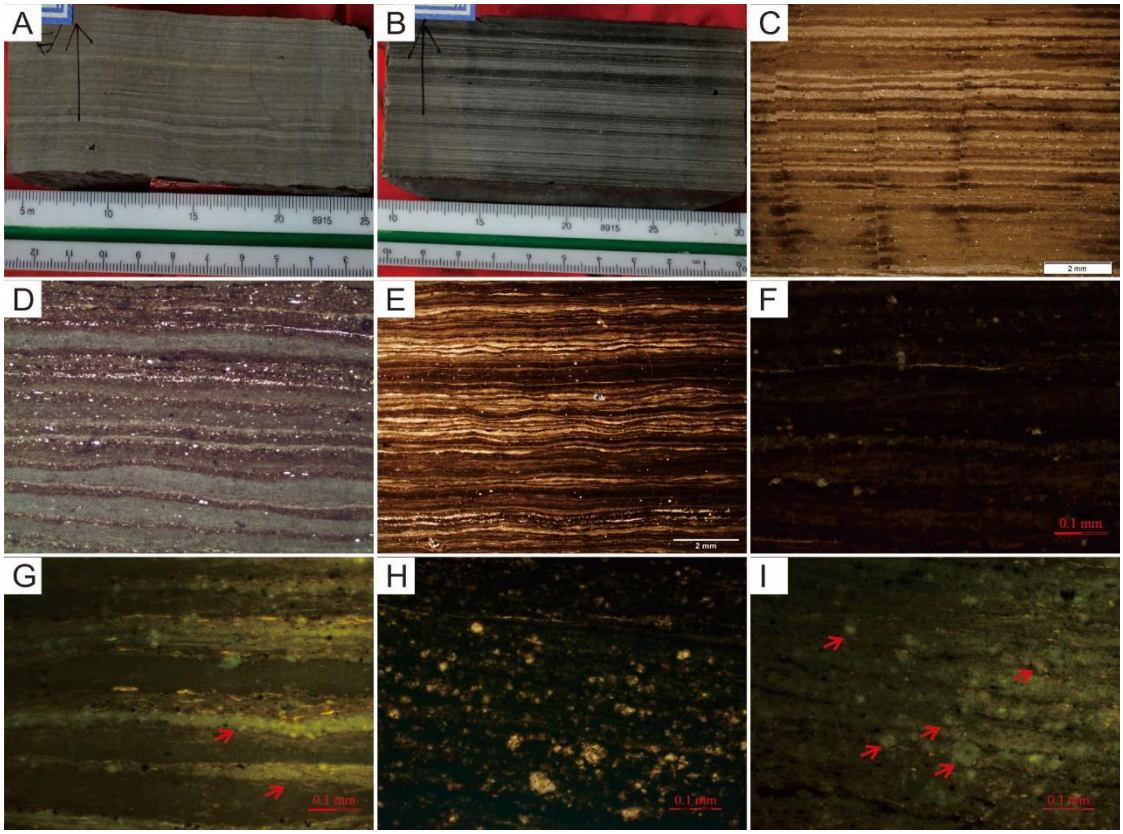

Figure 4. The micritic carbonates. A: well Niuye1, 3,401.20 m, core photo, interbedded mudstone and shale and micritic carbonates laminas, mudstone and shale is dark grey, micritic carbonate laminas are light color; B: well Fanye1, 3,412.14 m, core photo, interbedded mudstone and shale and micritic carbonates laminas; C: well Niuye1, 3,426.73 m, plane-polarized light, micritic carbonate laminas are horizontal, mineral crystals are difficult to distinguish; D: well Fanye1, 3,377.05 m, plane-polarized light, micritic carbonate laminas are horizontal; E: well Niuye1, 3,401.30 m, plane-polarized light, micritic carbonate laminas are microwave type; F: well Niuye1, 3,401.30 m, plane-polarized light, micritic carbonate laminas are horizontal; G: F under fluorescence, red arrows indicate whole micritic carbonate laminas that appear greenish; H: well Niuye1, 3,414.56 m, plane-polarized light, micritic carbonates as aggregations; I: H under fluorescence, red arrows indicate aggregations scattered within the micritic carbonates, which appear greenish.

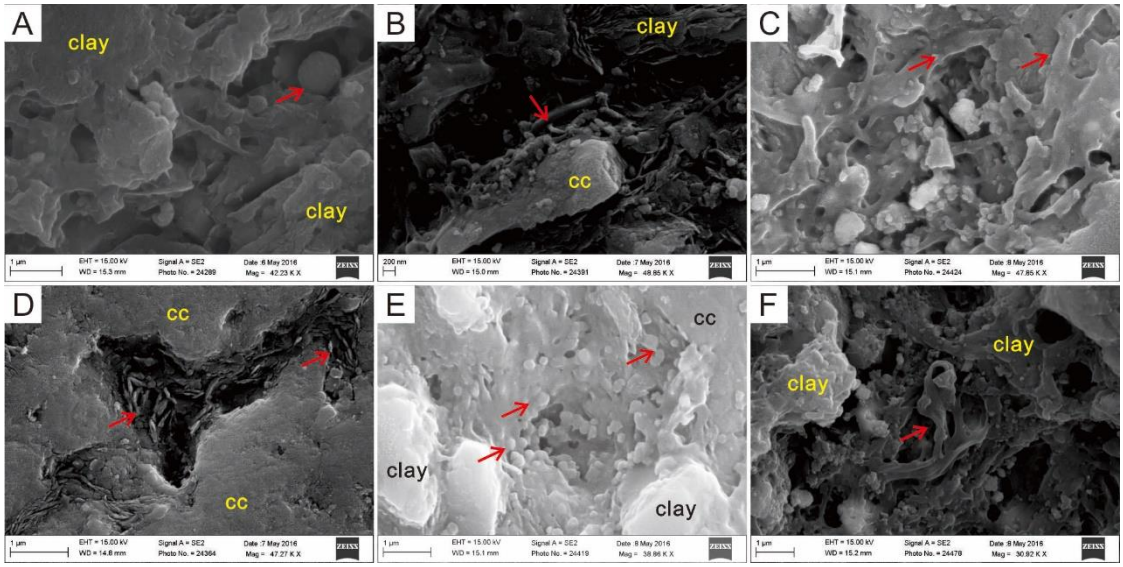

Figure 5. The SEM image of micritic carbonates. A: well Niuye1, 3,331.79 m, red arrow indicates spherical calcite; B: well Niuye1, 3,331.79 m, red arrow indicates calcite with sheath-like texture, adhered with surrounding minerals; C: well Fanye1, 3,412.14 m, red